Collisionless electron cooling on magnetized plasma expansions: advances on modelling

IEPC-2015-117/ISTS-2015-b-117

Presented at Joint Conference of 30th International Symposium on Space Technology and Science, 34th International Electric Propulsion Conference and 6th Nano-satellite Symposium
Hyogo-Kobe, Japan
July 4–10, 2015

Jaume Navarro-Cavallé* and Sara Correyero†
Universidad Politecnica de Madrid, Madrid, 28040, Spain

Eduardo Ahedo‡
Universidad Carlos III Madrid, Leganes, 28911, Madrid, Spain

This work inquires into the study of a steady-state, quasi-neutral, current-free and magnetized plasma flowing through a magnetic nozzle channel (quasi-1D). At the plasma reservoir, far upstream from the magnetic nozzle throat, electrons and ions are considered fully Maxwellian. Ion and electron distribution functions are solved consistently accounting for both magnetic mirror and potential barriers effects to find the electric potential ϕ - magnetic field B relation and the total potential drop. The solution is used to calculate the evolution of various moments along the expansion (density, fluxes, temperatures). A parametric analysis, as a function of the dimensionless driven parameters (ion to electron mass and source temperature ratios) identifies several fitting laws for the total potential drop and the bounded limit of the electron temperature. The evolution of the electron distribution function is analysed in depth to illuminate the electron collisionless cooling process.

I. Introduction

The properties of expanding weakly-collisional magnetized plasmas requires the understanding of some physical mechanisms that are crucial issues on the characterization of the propulsive performance of most of the existing plasma thrusters, especially on those that implement a magnetic nozzle to guide and accelerate the plasma jet. For instance, the helicon plasma thruster,[1–3] that uses a helicon source to produce and heat the plasma, which is then accelerated in a magnetic nozzle. Also, the VASIMR, similar to the helicon plasma thruster,[4,5] but including an Ion Cyclotron Resonance stage between the helicon source and the magnetic nozzle, or the Electron Cyclotron Resonance plasma thruster (ECR),[6] which consists on an ECR plasma source combined with a magnetic nozzle. These devices are some examples of the importance of understanding the dynamics of plasma expansions, and are the main motivation of this work.

One of the main concerns is due to the uncertainties on the temperature evolution and heat fluxes in nearly-collisionless plasmas, since predicting the electron temperature far downstream from the source is of particular interest when the distant plasma can be in contact with sensitive thruster surfaces. The problem lies in the closure of the fluid equation hierarchy, since in the absence of collisions, one is forced to

*PhD candidate, Universidad Politecnica de Madrid (EP2 member), jaume.navarro@upm.es
†PhD student, Universidad Politecnica de Madrid (EP2 member), Madrid, 28040, saracorreyeroplaza@gmail.com
‡Professor, Equipo de Propulsión Espacial y Plasmas (EP2), Universidad Carlos III de Madrid, Spain, eduardo.ahedo@uc3m.es

adopt electron temperature models, and most of the existent models of plasma plumes assume isothermal or polytropic laws. An isothermal assumption is only justifiable if the distribution remains close to Maxwellian, and fails to predict a finite total potential drop along the plume (consequently leads to unbounded acceleration of the plasma). Moreover, adiabatic models cannot be justified in the collisionless regime, and polytropic laws are just empirical fittings.[7] Some modellers have already shown that a steady collision-free expansion is possible,[8] as well as the importance of considering a trapped electron population possibly developed during the start-up transient. However, these simulations do not fully disclose all the mechanisms involved.

This paper is based on the work performed in Ref.9, which formulates a steady-state, collisionless, quasi-neutral slender flow of a magnetized plasma model, assuming Maxwellian electrons and mono-energetic ions at the source, and it solves consistently the axial evolution of the electric potential and the electron/ion distribution functions. Here, ions are postulated Maxwellian at the source instead of mono-energetic, and it is performed an exhaustive analysis of the evolution of the electron distribution function along the expansion. This way, different electron populations are identified in order to characterize the electron cooling law given by this model.

The model formulation is briefly summarized in Section II. Section III shows and discusses the results from the Maxwellian distribution model, including a comparison with the solution obtained in Ref.9 for mono-energetic ions. The evolution of the electron distribution function is discussed in Section IV. Fitting laws for the electron cooling process are determined as well in Section V. Finally, Section VI summarizes the conclusions of the study.

II. Model formulation

An externally applied magnetic field $B(z)$ vanishing at $z = \pm\infty$ and with a single maximum B_M located at $z = 0$, generates a convergent-divergent magnetic nozzle that channels an ion/electron plasma created at $z = -\infty$. The model here attempts to determine the quasi-1D (i.e. paraxial), steady-state response of the plasma beam which is assumed collisionless, quasineutral, current-free (i.e. zero electrical current is transported), and fully-magnetized everywhere (of course, the last feature becomes an asymptotic idealization far upstream and downstream, when the magnetic field vanishes). Figure 1 sketches the geometry and some characteristics of the model. Subscripts '0' and '∞' will be used for $z = -\infty$ and $z = \infty$.

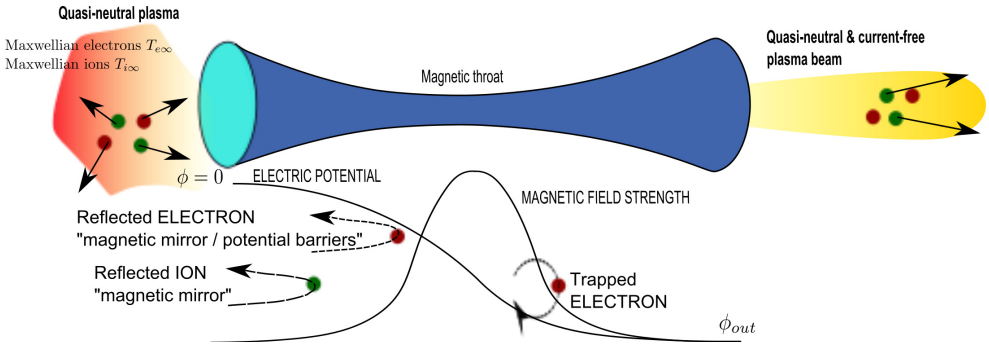

Figure 1. Sketch of the problem describing the geometry and introducing some hypotheses and phenomena.

Particle-drift and induced-field effects of the magnetic field are totally disregarded. The different ion and electron dynamics plus plasma quasineutrality and zero-current, set the profile $\phi(z)$ of the ambipolar electric potential. It is assumed (and then confirmed by the solution) that $\phi(z)$ decreases monotonically along the nozzle. We set $\phi(-\infty) = 0$ and call $\phi(+\infty) = \phi_\infty (< 0)$; this total potential fall along the nozzle is going to be a central output of the model.

As a consequence of fully-magnetization and lack of collisions, electron and ions ($\alpha = i, e$) conserve their total energy and their magnetic moment,

$$E_\alpha = \frac{m_\alpha}{2}(w_{\alpha\parallel}^2 + w_{\alpha\perp}^2) + q_\alpha \phi, \tag{1}$$

$$\mu_\alpha = \frac{m_\alpha w_{\alpha\perp}^2}{2B} \tag{2}$$

where $q_i = e$, $q_e = -e$, and $w_{\alpha\parallel}$ and $w_{\alpha\perp}$ are the velocity components parallel and perpendicular to B, respectively. In terms of the invariants of motion, these components are expressed as

$$w_{\alpha\parallel}(z, E_\alpha, \mu_\alpha) = \pm\sqrt{\frac{2}{m_\alpha}\left[E_\alpha - q_\alpha\phi(z) - \mu_\alpha B(z)\right]} \tag{3}$$

$$|w_{\alpha\perp}(z, \mu_\alpha)| = \sqrt{\frac{2\mu_\alpha B(z)}{m_\alpha}} \tag{4}$$

Condition $w_{\alpha\parallel} = 0$, sets a maximum magnetic moment for each energy and location:

$$\mu_{im}(z, E_e) = \frac{E_i - e\phi(z)}{B(z)}, \quad \mu_{em}(z, E_e) = \frac{E_e + e\phi(z)}{B(z)}, \tag{5}$$

such that at a given z there are not particles with $\mu_\alpha > \mu_{\alpha m}(z, E_\alpha)$. Since $d\phi/dz < 0$ at any z and $\text{sign}(dB/dz) = \text{sign}(-z)$, it turns out that $\mu_{im}(z; E_i)$ is spatially monotonic at $z > 0$ but can have extrema at $z < 0$, while the opposite is true for $\mu_{em}(z; E_e)$. Hereafter, we postulate (and results will confirm) that $\mu_{im}(z; E_i)$ presents a single minimum $\mu_{iT}(E_i)$ at $z = z_{iT}(E_i) < 0$ (in the convergent nozzle), and $\mu_{em}(z; E_e)$ presents a single minimum $\mu_{eT}(E_e)$ at $z = z_{eT}(E_e) > 0$ (in the divergent nozzle).

With these postulates, ions from the upstream source can be split in two groups: *free ions*, having $\mu_i \leq \mu_{iT}(E_i)$, and reaching $z = +\infty$, and *reflected/confined ions*, having $\mu_i > \mu_{iT}(E_i)$; notice that there are only free ions in the divergent nozzle. Electrons from the upstream source, can be split into *free electrons*, having $E_e > e|\phi_\infty|$ and $\mu < \mu_{eT}(E_e)$, and *reflected electrons*, otherwise. In addition there could be a population of *trapped electrons*, with $E_e^* < E_e < e|\phi_\infty|$, unconnected to the upstream source, which bounce back and forward in a region $z_{eT}(E_e) < z < z'_{eT}(E_e)$ within the divergent nozzle, with $z'_{eT}(E_e)$ the solution of $\mu(z'_{eT}, E_e) = \mu_{eT}(E_e)$ and E_e^* the solution of $d^2\mu_{em}(z_{eT}(E_e^*); E_e^*)/dz^2 = 0$. In short, electrons present throughout the expansion can be split into two main groups: *free* or *confined*. Then, *confined* electrons are in turn divided into two different populations: *trapped* or *reflected*, and finally we distinguish between *reflected* electrons of *high energy* with $E_e > e|\phi_\infty|$ and *low energy*, otherwise.

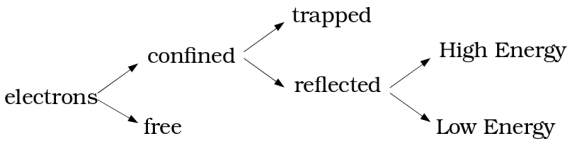

Figure 2. Different types of electrons present in the expansion

These existence limits for the different electron populations are shown in Table 1. Fig.3 represents the maximum local magnetic moment μ_{em} for three energies: 'a' belongs to $E_e < E_e^*$, where it is shown how electrons with this energy would be necessarily bounced back at some point of the expansion, 'b' belongs to $E_e^* < E_e < e|\phi_\infty|$, where we can see the existence of a minimum and a maximum of μ_{em} and the region of trapped electrons is clearly identified, and finally 'c' belongs to $E_e > e|\phi_\infty|$, where electrons can escape and neutralize ions if they have a magnetic moment higher than μ_{eT}.

Population	lower E_e	upper E_e	lower μ_e	upper μ_e
F-Free	$-e\phi_\infty$	∞	0	μ_{eT}
T-Trapped	E_e^*	$-e\phi_\infty$	μ_{eT}	μ_{em}
RH-Reflected high	$-e\phi_\infty$	∞	μ_{eT}	μ_{em}
RL-Reflected low	$-e\phi$	$-e\phi_\infty$	0	μ_{em} or μ_{eT}

Table 1. Existence limits for the different electron populations

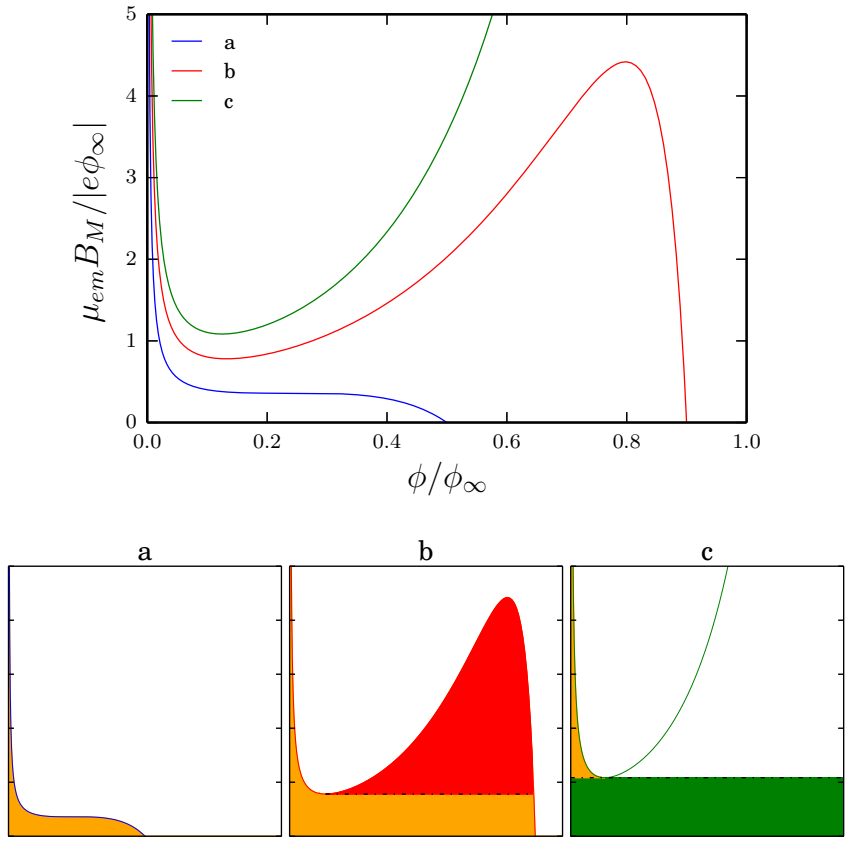

Figure 3. The maximum local magnetic moment, $\frac{\mu_{em}B_M}{|e\phi_\infty|}$, versus potential drop, $\frac{\phi}{\phi_\infty}$, for various electron energies, "a, b, c" correspond to $E_e/|e\phi_\infty| = [0.5, 0.9, 1.2]$ respectively. These results are for $T_{i0}/T_{e0} = 0.1$ and $m_i/m_e = 10000$. Subfigures "a,b and c" represent the same curves coloured, showing the different electron populations for each case (yellow:reflected, green:free, red:trapped).

The trapped population can be formed in the initial transient formation of the stationary response or due to infrequent electron collisions. Following Ref.9, here we will assume that the distribution function of trapped electrons has the same functional dependence than electrons coming from the upstream source.

In a collisionless plasma, the distribution function of each species is a function of the motion invariants and $\phi(z)$ and $B(z)$ and requires only to set the distribution function of forward-marching particles, at $z = -\infty$, $f_{\alpha+}(E_\alpha, \mu_\alpha)$.

Fig.4 represents the electron distribution function in terms of the two motion invariants at two different local positions (convergent and divergent side), where there are perfectly distinguishable the four types of electrons present on the expansion.

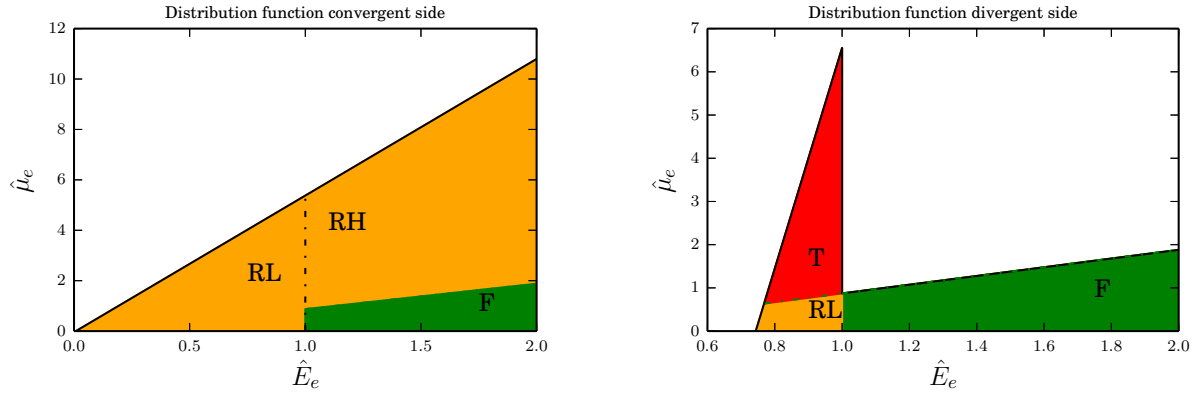

Figure 4. Electron distribution function for the profile $m_i/m_e = 10000$ and $\frac{T_{i0}}{T_{e0}} = 1.0$ at two different local positions, $\frac{\phi}{\phi_\infty} = 0.05$ for the convergent region and $\frac{\phi}{\phi_\infty} = 0.72$ for the divergent region. "RH" represents the high energy reflected electrons, "RL" stands for the low energy reflected electrons, "F" corresponds to the free electron population and finally "T" represents the trapped electrons (only existing in the divergent region of the expansion)

Macroscopic variables are computed in the standard way, taking integral moments of the distribution function according to

$$\langle \chi_\alpha \rangle(z) = \frac{2\pi B(z)}{m_\alpha^2} \int\int \chi_\alpha(E_\alpha, \mu_\alpha) \frac{f_{\alpha+}(E_\alpha, \mu_\alpha)}{|w_{\alpha\parallel}|(z)} dE_\alpha d\mu_\alpha, \tag{6}$$

where: we used that the differential volume in the velocity space in terms of E_α and μ_α, with symmetry about the magnetic line, is $dE_\alpha d\mu_\alpha 2\pi B/\left(m_\alpha^2 |w_{\alpha\parallel}|\right)$; boundaries on the integration domain are set according to the previous discussion on confined and free particles; and confined particle contribution includes both forward and backward marching ones. Then,

$$n_\alpha \equiv \langle 1 \rangle, \quad \Gamma_\alpha \equiv n_\alpha u_\alpha \equiv \langle w_{\alpha\parallel} \rangle, \quad P_{\alpha\parallel} = n_\alpha k T_{\alpha\parallel} \equiv \langle m_\alpha c_{\alpha\parallel}^2 \rangle, \quad P_{\alpha\perp} = n_\alpha k T_{\alpha\perp} \equiv \langle \frac{m_\alpha c_{\alpha\perp}^2}{2} \rangle = B \langle \mu_\alpha \rangle$$

The ambipolar electric potential $\phi(z)$ is included in $w_{\alpha\parallel}$ and the integral limits of Eq.6. Therefore, species densities and the rest of macroscopic variables are composed functions $n_\alpha(z, \phi(z))$. The self-consistent solution for the electric potential comes from solving the quasineutrality integral equation

$$n_i(B(z), \phi(z)) = n_e(B(z), \phi(z)), \tag{7}$$

It can be shown that $|\phi_\infty|$ is a free parameter of this equation, which is determined from imposing locally the zero current condition

$$\Gamma_i - \Gamma_e = 0. \tag{8}$$

The extension of the present model to current-carrying plasmas is straightforward and will not be discussed here.

III. Solution for initially Maxwellian isotropic ions and electrons

The work here is an extension of the one performed in Ref.9, where, at the source, electrons were postulated Maxwellian and ions constitute a mono-energetic population. Here, both electrons and ions are postulated Maxwellian at the source. According to this, the upstream ion and electron distribution functions are

$$f_i(E_i, w_{i\parallel} > 0) = n_0 \left(\frac{m_i}{2\pi k T_{i0}}\right)^{3/2} \exp\left(\frac{-E_i}{k T_{i0}}\right), \tag{9}$$

$$f_e(E_e, w_{e\parallel} > 0) = n_0 \left(\frac{m_e}{2\pi k T_{e0}}\right)^{3/2} \exp\left(\frac{-E_e}{k T_{e0}}\right), \tag{10}$$

It will be found that both f_i and f_e are practically Maxwellian at $z \to -\infty$ so that n_0 is the upstream plasma density. Regarding ions, the energy integration limits in Eq.6 are $[0, \infty]$. For $z > z_{iT}(E_i)$, the magnetic moment limits are $[0, \mu_{iT}]$. These ions are counted only once, since they are travelling only in the forward direction (free ions). For $z < z_{iT}(E_i)$ the μ_i range must be split: For $0 < \mu_i < \mu_{iT}$ ions are counted once (free) and for $\mu_{iT} < \mu_i < \mu_{im}$ ions must be accounted in both forward and backward directions (reflected ions). The expression for the ion density is then

$$\frac{n_i(z)}{n_0} = \frac{1}{\sqrt{\pi}\left(kT_{i0}\right)^{3/2}} \int_0^\infty e^{-(E_i/kT_{i0})} \left(\sqrt{E_i - e\phi} + \text{sign}[z_{iT}(E_i) - z] \sqrt{E_i - e\phi - \mu_{iT}(E_i)B} \right) dE_i \tag{11}$$

Concerning the electrons, integration limits in Eq.6 are defined according to Tab.1, where for all confined populations a factor of two is needed to account for returning electrons. Substituting $\alpha = e$ and $\chi = 1$ in Eq.6 with its respective limits for each electron population and solving the integrals, the electron density equation can be regrouped and presented as

$$\frac{n_e(z)}{n_0} = e^{\left(\frac{e\phi}{kT_{e0}}\right)} \text{erf}\sqrt{\frac{e\left(\phi - \phi_\infty\right)}{kT_{e0}}} - \frac{2}{\sqrt{\pi}} e^{\left(\frac{e\phi_\infty}{kT_{e0}}\right)} \sqrt{\frac{e\left(\phi - \phi_\infty\right)}{kT_{e0}}} +$$

$$\frac{1}{\sqrt{\pi}\left(kT_{e0}\right)^{3/2}} \int_{-e\phi_\infty}^\infty \left(\sqrt{E_e + e\phi} + \text{sign}[z_{eT}(E_e) - z] \sqrt{E_e + e\phi - \mu_{eT}B} \right) e^{-\left(\frac{E_e}{kT_{e0}}\right)} dE_e \tag{12}$$

For $z > z_{eT}(E_e)$ the integral term in Eq.12 stands only for the *free* electron population, while for $z < z_{eT}(E_e)$ it represents both *free* and *reflected high energy* electrons. The rest of the terms in Eq.12 represent the remaining confined electrons (both *trapped* and *reflected low energy*).

The net current is given by combining the ion and electron fluxes, Γ_i and Γ_e, resulting

$$\frac{\Gamma_i}{B} = \frac{n_0}{\sqrt{2\pi}\sqrt{m_i}\left(kT_{i0}\right)^{3/2}} \int_0^\infty \mu_{iT}(E_i) e^{\left(-\frac{E_i}{kT_{i0}}\right)} dE_i = const \tag{13}$$

$$\frac{\Gamma_e}{B} = \frac{n_0}{\sqrt{2\pi}\sqrt{m_e}\left(kT_{e0}\right)^{3/2}} \int_{-e\phi_\infty}^\infty \mu_{eT}(E_e) e^{\left(-\frac{E_e}{kT_{e0}}\right)} dE_e = const \tag{14}$$

The quasineutrality condition formulated with Eq.11 and Eq.12 contains an implicit relation of $\phi(B)$. To solve the problem we normalize the variables as follows:

$$\hat{B} = \frac{B}{B_M}, \quad \hat{\phi} = -\frac{e\phi}{kT_{e0}}, \quad \hat{\mu}_\alpha = \frac{\mu_\alpha B_M}{kT_{\alpha 0}}, \quad \hat{E}_\alpha = \frac{E_\alpha}{kT_{\alpha 0}}, \quad \hat{T}_\alpha = \frac{T_\alpha}{T_{\alpha 0}}, \quad \hat{n}_\alpha = \frac{n_\alpha}{n_0}, \quad \hat{u}_\alpha = \frac{u_\alpha}{c_{s0}}$$

where B_M represents the magnetic field strength at the magnetic throat, and c_{s0} stands for the ion sonic velocity, so $c_{s0} = \sqrt{kT_{e0}/m_i}$.

The quasineutrality and current-free conditions can be now written in non-dimensional form as

$$\frac{1}{\sqrt{\pi}} \int_0^\infty e^{-\hat{E}_i} \left(\sqrt{\hat{E}_i + \frac{T_{e0}}{T_{i0}}\hat{\phi}} + \text{sign}[z_{iT} - z] \sqrt{\hat{E}_i + \frac{T_{e0}}{T_{i0}}\hat{\phi} - \hat{\mu}_{iT}\hat{B}} \right) d\hat{E}_i = e^{-\hat{\phi}} \text{erf}\sqrt{\hat{\phi}_\infty - \hat{\phi}}$$

$$-\frac{2}{\sqrt{\pi}} e^{-\hat{\phi}_\infty} \sqrt{\hat{\phi}_\infty - \hat{\phi}} + \frac{1}{\sqrt{\pi}} \int_{\hat{\phi}_\infty}^\infty \left(\sqrt{\hat{E}_e - \hat{\phi}} + \text{sign}[z_{eT} - z] \sqrt{\hat{E}_e - \hat{\phi} - \hat{\mu}_{eT}\hat{B}} \right) e^{-\hat{E}_e} d\hat{E}_e \tag{15}$$

$$\int_{\hat{\phi}_\infty}^\infty \hat{\mu}_{eT} e^{-\hat{E}_e} d\hat{E}_e = \sqrt{\frac{m_e}{m_i}} \sqrt{\frac{T_{i0}}{T_{e0}}} \int_0^\infty \hat{\mu}_{iT} e^{-\hat{E}_i} d\hat{E}_i \tag{16}$$

As it is shown in Eq.15 and Eq.16, two dimensionless parameters drive the problem: The ion to electron mass ratio m_i/m_e and the ion to electron temperature ratio T_{i0}/T_{e0}. Eq.15 is an integral equation for $\hat{\phi}\left(z, \hat{\phi}_\infty, \frac{T_{i0}}{T_{e0}}\right)$ and Eq.16 provides $\hat{\phi}_\infty\left(\frac{m_i}{m_e}, \frac{T_{i0}}{T_{e0}}\right)$.

To solve the problem, an iterative method is implemented following the scheme presented in Ref.9.

A. Results compared with the ion mono-energetic case

This section presents the main results of the model, comparing them with the solution obtained by postulating mono-energetic ions at the source instead of Maxwellian.[9] It presents $\hat{\phi}(\hat{B})$ and the evolution of plasma density and ion Mach number along the expansion (depicted against the potential $\hat{\phi}$). The evolution of ion and electron temperatures is computed and analysed in terms of the two dimensionless parameters that control the plasma expansion, the ion to electron source temperature ratio and the mass ratio.

To make a comparison between the two models, we establish a relation between the ion energy dimensionless parameter in Ref.9 and the ion to electron source temperature ratio defined in this work, as it is shown in Eq.17. Notice that in Ref.9 the ion energy is normalized with the electron temperature at the source, therefore it is different from the ion energy parameter defined here, normalized with the ion source temperature instead.

$$\Theta = \frac{kT_{i0}}{kT_{e0}} = \frac{2}{3}\frac{E_{i0}}{kT_{e0}}, \tag{17}$$

The first result is the evolution of the electric potential $\hat{\phi}(\hat{B})$, which is represented in Fig.5, as well as the total potential drop $\hat{\phi}_\infty$, for a fixed mass ratio $m_i/m_e = 10000$ and different values of the ion to electron source temperature ratio Θ. As it can be observed, the solution is hardly different from the mono-energetic case, although it is possible to appreciate a greater deviation of the total electric potential drop $\hat{\phi}_\infty$ for higher values of Θ. The total potential drop is directly related to the current-free equation, which in turn depends on the two dimensionless parameters (mass and source temperature ratios).

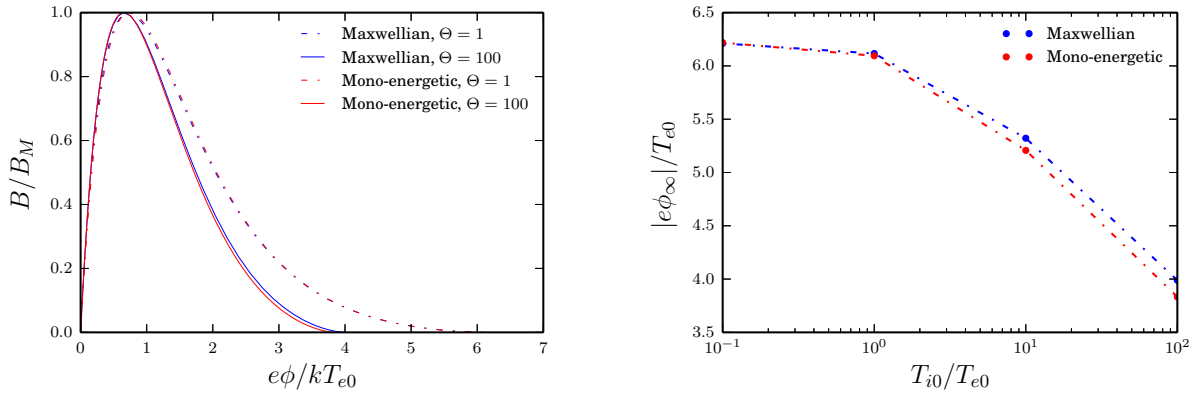

Figure 5. Dimensionless magnetic field as a function of normalized electric potential, for two values of the ion to electron source temperature ratio $\Theta = T_{i0}/T_{e0}$ and a fixed mass ratio $m_i/m_e = 10000$ for the mono-energetic and Maxwellian ion solution. Final value of the dimensionless electric potential drop $\hat{\phi}_\infty$ for several Θ values.

Once the evolution of the electric potential along the expansion $\hat{\phi}(\hat{B})$ and the total potential drop $\hat{\phi}_\infty$ are determined, moments of the distribution functions are computed in order to calculate macroscopic variables (density, temperatures...).

Figures 6 and 7 represent certain magnitudes, compared with the ion mono-energetic case for a fixed mass-ratio $m_i/m_e = 10000$ and for two different values of the ion to electron source temperature ratio($T_{i0}/T_{e0} = 1$ and $T_{i0}/T_{e0} = 100$).

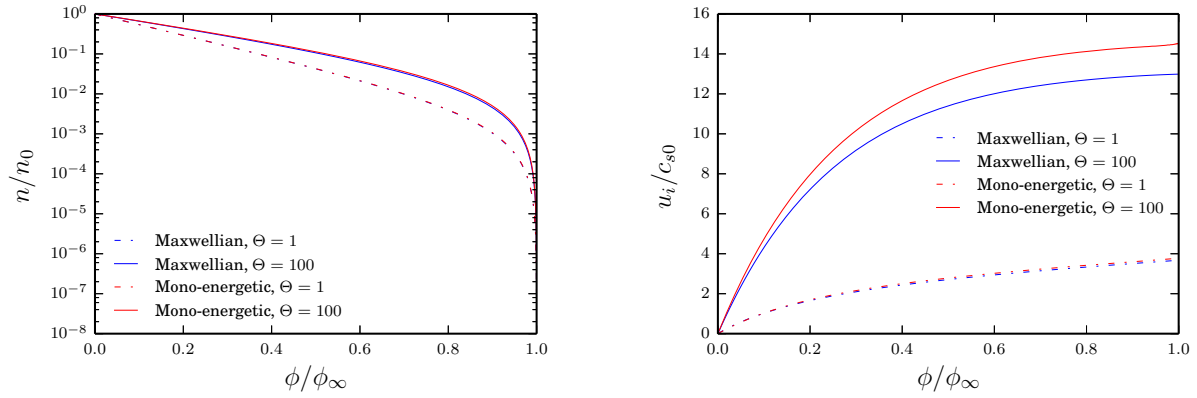

Figure 6. Dimensionless plasma density and ion speed as functions of normalized electric potential, for two values of the ion to electron source temperature ratio $\Theta = T_{i0}/T_{e0}$ for the mono-energetic and Maxwellian ion solution.

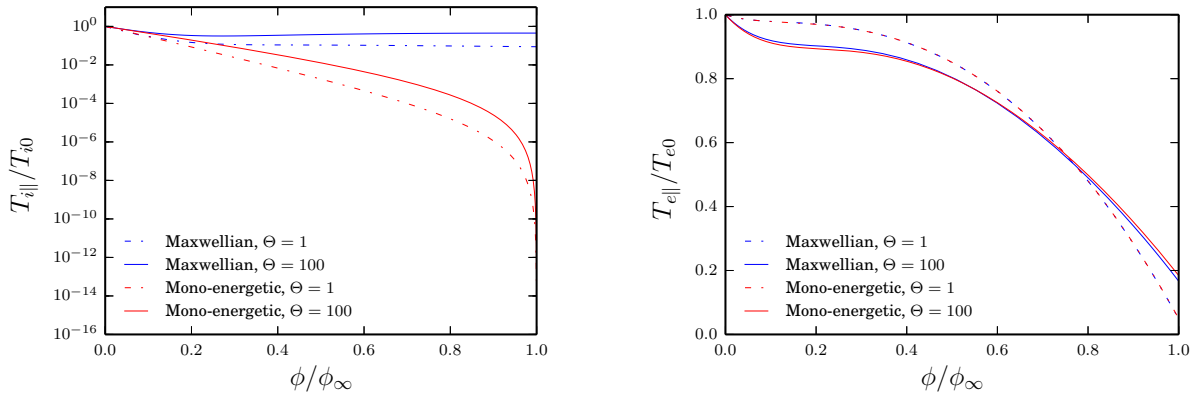

Figure 7. Ion and electron parallel temperatures as functions of normalized electric potential, for two values of the ion to electron source temperature ratio $\Theta = T_{i0}/T_{e0}$ for the mono-energetic and Maxwellian ion solution.

Plasma density and ion Mach number are depicted against the electric potential in Fig.6, where it is shown that while plasma density does not present any noticeable difference with the mono-energetic solution, the final ion Mach number is higher in the mono-energetic case for a high value of the ion to electron source temperature ratio ($\Theta = 100$). This difference is already predictable once $\hat{\phi}_\infty$ has been compared, since the ion acceleration is directly related to the total electric potential drop.

Ion and electron parallel temperatures are analysed and depicted in Fig.7. As it was expected, the ion temperature law changes. This is due to the distribution function postulated at the source, since while a mono-energetic distribution leads to a zero temperature at the end of the expansion, a Maxwellian distribution keeps an energy dispersion. The existence of this phenomenon can be justified by the conservation of each particle magnetic moment. This forces the perpendicular kinetic energy to drop to zero when the magnetic field intensity approximates zero as well. Consequently, particles with the same total energy (mono-energetic case) would necessarily have the same parallel kinetic energy at the end of the expansion, expecting the final parallel temperature to be zero, while a population with an energy distribution would not suffer this effect. It can be deduced from Fig.7 that at the convergent region, the mono-energetic solution for ion temperature is very similar to the one obtained for Maxwellian ions, starting to separate at the magnetic throat and being completely different at the divergent side of the expansion. However, the electron temperature, and consequent electron cooling, is not practically affected in this case by the ion distribution function.

IV. Discussion of the different electron populations

In order to characterise the different electron populations, as well as the electron temperature law, a study of the electron behaviour is performed in this section with the results for mono-energetic ions (electron behaviour is analogous for the ion-Maxwellian distribution solution, as it was shown in Sec.III). The electron population loses its isotropy since the beginning of the expansion, already at the convergent region, so parallel and perpendicular temperatures are analysed separately, paying more attention to the parallel one, since it is the flow direction. Electrons will be sorted as three different populations: *free*, *reflected (low and high)* and *trapped*, according to their behaviour in the expansion (See Fig.2).

A. Contribution to the total plasma density

Fig.8 left shows the contribution of the different electron populations to the total density along the expansion (the expansion is from right to left). At the convergent side, density is dominated by reflected electrons (there are no trapped electrons and the free ones influence barely the solution). An interesting fact is that the influence of the trapped electrons is very noticeable since they appear at a certain location of the divergent side, coming to dominate and guide the final expansion. Fig.8 right shows the final value achieved downstream by the confined electrons of the partial contribution to total density ratio, for different mass ratio values. As it can be noticed, the free electron population never contributes more than the confined electrons for all the simulated cases in this work. This is due to the distribution function of each population; while confined electrons present an isotropic velocity distribution, free electrons contribute as a "beam" in the velocities space, what leads confined electrons to weigh more in the total density calculation.

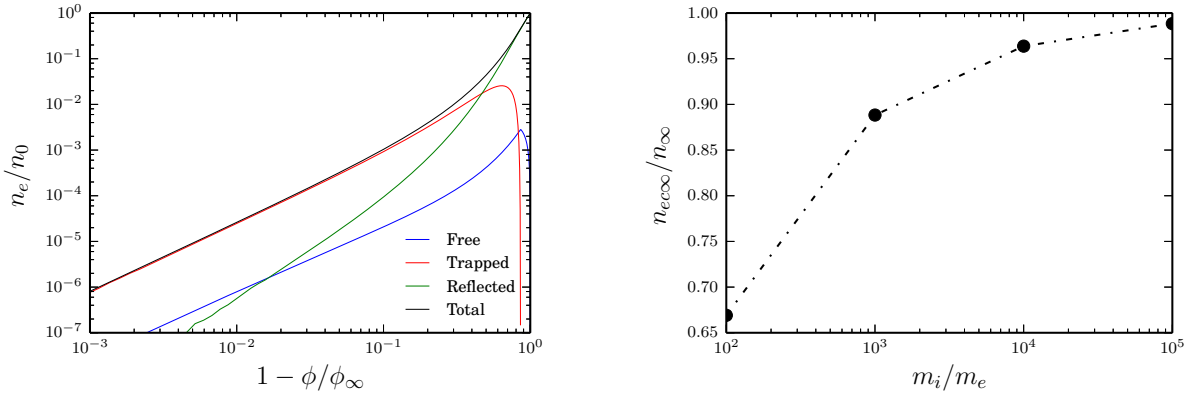

Figure 8. Contribution to the total density of each electron population along the expansion (left) and the ratio between the final confined electron density $n_{ec\infty}$ and the final total density n_∞ for different mass ratio profiles (right).

B. Contribution to parallel and perpendicular pressures

Considering the three electron populations sorted here, *free (F)*, *reflected (R)* and *trapped (T)*, we can define a partial pressure due to the different types of electrons, in such a way that the sum of all these partial contributions is the total electron pressure.

$$P_e = P_{eF} + P_{eR} + P_{eT} \tag{18}$$

Fig.9 shows the contribution to the total parallel and perpendicular pressure of each electron population in terms of the electric potential (The expansion is from right to left). Results for perpendicular pressure are similar to the ones obtained for the total density: Free electrons contribute poorly while trapped electrons dominate the final expansion region. More interesting is the contribution to the total parallel pressure, since there are three regions clearly defined. First, reflected electrons govern the total pressure. Then, there is a transition region that leads to the domination of the trapped electrons population. This population governs the parallel pressure until the tail of the Maxwellian distribution (free electrons) ends up dominating the expansion.

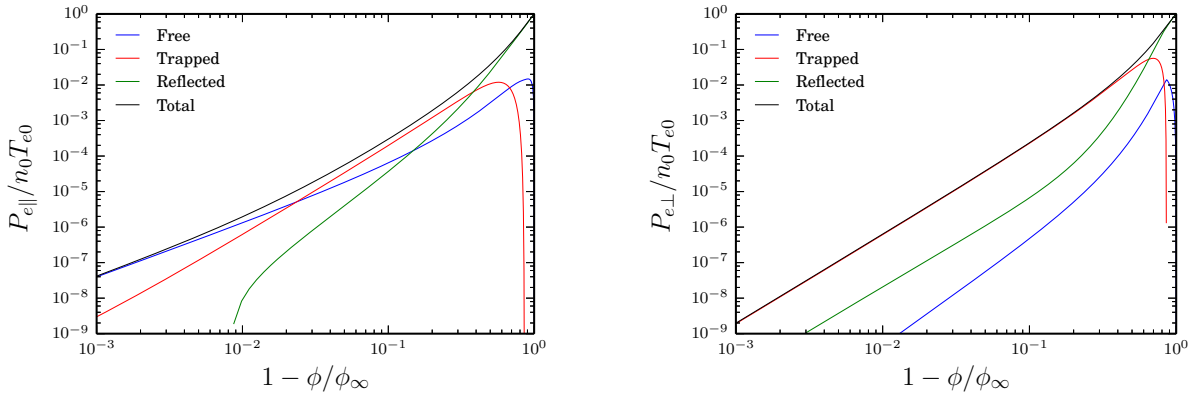

Figure 9. Contribution to parallel and perpendicular electron pressure of each electron population (free, trapped and reflected) along the expansion (from right to left). Solution for the profile $T_{i0}/T_{e0} = 1$ and $m_i/m_e = 10000$.

C. Trapped and low energy reflected population

The importance of the confined electron population (trapped plus reflected) has been discussed in IV.A and IV.B, where density and pressure have been plotted in terms of different electron contributions. In this subsection, trapped and reflected of low energy electrons are analysed as an unique isolated population (subscript "ec"), where different moments are computed as

$$n_{ec} = \int f_{ec}(\vec{w})d\vec{w}, \quad P_{ec} \equiv n_{ec}T_{ec} = \int m_e w_\parallel^2 f_{ec}(\vec{w})d\vec{w}, \quad \Gamma_{ec}, u_{ec} = 0$$

The definitions above lead to analytical expressions for both density and temperature (parallel and perpendicular temperature behave the same way in this population).

$$\hat{n}_{ec}(\hat{\phi}) = e^{-\hat{\phi}}\mathrm{erf}\sqrt{\hat{\phi}_\infty - \hat{\phi}} - \frac{2}{\sqrt{\pi}}e^{-\hat{\phi}_\infty}\sqrt{\hat{\phi}_\infty - \hat{\phi}} \tag{19}$$

$$\hat{T}_{ec}(\hat{\phi}) = \frac{2}{\sqrt{\pi}\hat{n}_{ec}}\left(\frac{\sqrt{\pi}}{2}e^{-\hat{\phi}}\mathrm{erf}\sqrt{\hat{\phi}_\infty - \hat{\phi}} + \frac{e^{-\hat{\phi}_\infty}}{3}\sqrt{\hat{\phi}_\infty - \hat{\phi}}\left(2\left(\hat{\phi} - \hat{\phi}_\infty\right) - 3\right)\right) \tag{20}$$

The expressions above can be evaluated at the end of the expansion when $\hat{\phi} \to \hat{\phi}_\infty$. The final density is obtained directly form Eq.19, resulting to be zero, but the final temperature value is a priori undetermined. However, because it is an analytical expression for the electric potential, its limit can be easily calculated applying L' Hôpital's rule.

$$\hat{T}_{ec\infty} = \lim_{x\to 0}\frac{\left(e^{\hat{\phi}_\infty x}\mathrm{erf}\sqrt{\hat{\phi}_\infty x} - \frac{2}{\sqrt{\pi}}\sqrt{\hat{\phi}_\infty x} - \frac{4}{3\sqrt{\pi}}(\hat{\phi}_\infty x)^{3/2}\right)}{e^{\hat{\phi}_\infty x}\mathrm{erf}\sqrt{\hat{\phi}_\infty x} - \frac{2}{\sqrt{\pi}}\sqrt{\hat{\phi}_\infty x}} = 0 \tag{21}$$

This result verifies that this electron population is not isothermal, but its temperature drops to zero at the end of the expansion. In this model, the loss of temperature along the expansion is governed by the confined electrons, since they weigh much more in density, while free electrons are responsible for the loss of isotropy and the final parallel temperature value, which is not zero, but a specific value depending on the driven parameters, whose dependency is analysed in the following section.

V. Fitting laws and parametric variations

As it has been presented in the formulation of the model, two parameters drive the problem: the mass ratio m_i/m_e and the ion to electron source temperature ratio T_{i0}/T_{e0}. In this section we study the impact of these parameters on some of the variables.

A. Parametric variations

The total drop of electric potential $\hat{\phi}_\infty$, as it was anticipated in Section III.A, is directly related to the two parameters, m_i/m_e and T_{i0}/T_{e0}, through the current-free equation (See Eq.16).

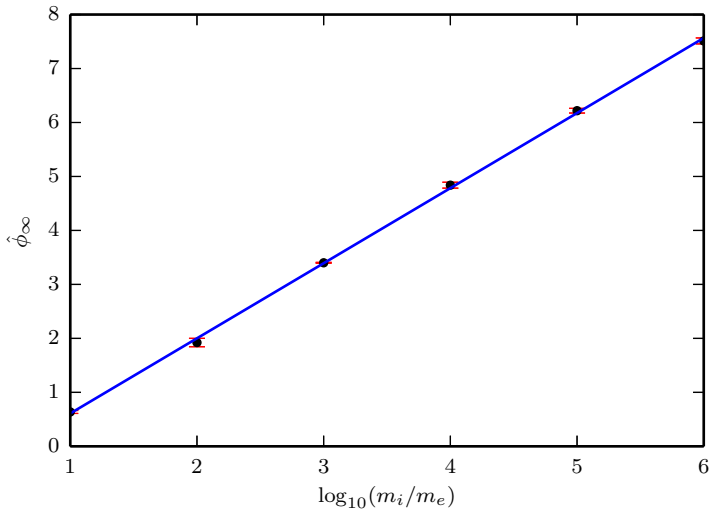

Figure 10. Total electric potential drop $\hat{\phi}_\infty$ for different ion to electron mass ratios $log_{10}(m_i/m_e) = [1-6]$. Linear approach (blue) with its error bars (red).

$$\hat{\phi}_\infty = 1.4 \log\left(\frac{m_i}{m_e}\right) + 0.78, \quad \text{for} \quad \left(\frac{T_{i0}}{T_{e0}} \leq 1\right) \tag{22}$$

For ions less energetic than electrons at the source ($T_{i0}/T_{e0} \leq 1.0$), the total electric potential drop $\hat{\phi}_\infty$ only depends on the mass ratio parameter (see Fig.5). Furthermore, it results to follow a linear trend with the logarithm of the ion to electron mass ratio parameter $\log(m_i/m_e)$, as it is written in Eq.22. Fig10 represents the final electric potential $\hat{\phi}_\infty$ for different mass ratio values overlapped with this linear fitting law.

Regarding the ion to electron source temperature ratio, its influence on the total drop of electric potential was already plotted in Fig.5. For higher values of T_{i0}/T_{e0}, the total drop of electric potential is smaller. This is due to the current-free condition (Eq.16), where it is noticeable that the dimensionless ion flux increases for higher T_{i0}/T_{e0} values, and therefore the total drop of electric potential must be reduced to increase the electron current and allow the fulfilment of this condition.

$$log_{10}(\hat{T}_{e\|\infty}) = -0.329\hat{\phi}_\infty + 0.707 \tag{23}$$

The final electron temperature is parametrically investigated within the studied range $m_i/m_e = [1000, 10000, 100000]$, which would include, for instance, the real cases of Xenon or Argon among others, it is found numerically a linear relation between the final electron temperature and the mass ratio, that combined with the linear relation founded between the total potential drop and the logarithm of the mass ratio (Eq.22) leads to a direct relation between the total potential drop and the final electron temperature (Eq.23).

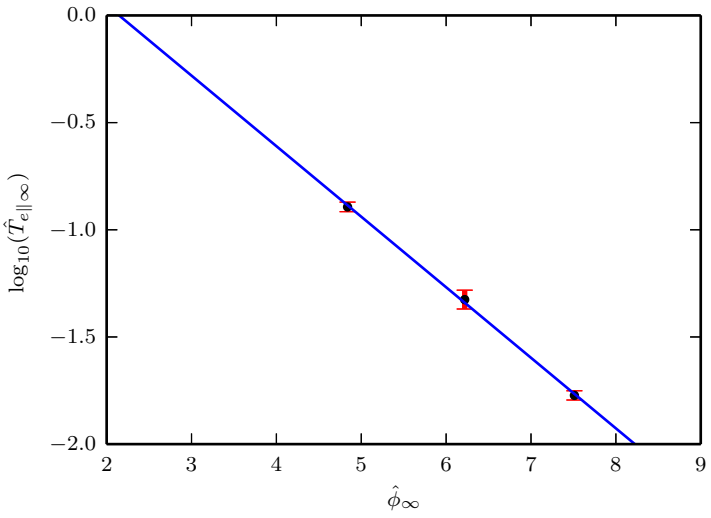

Figure 11. Logarithm of the final electron temperature $\hat{T}_{e\|\infty}$ against the total potential drop $\hat{\phi}_\infty$ for different ion to electron mass ratios $m_i/m_e = [1000, 10000, 100000]$. Linear approach (blue) with its error bars (red).

B. Fitting law for the electron temperature

The final electron temperature has been plotted in Fig.12 against the plasma density in order to study possible polytropic fittings. As it is shown in this Figure, the electron cooling law can be separated in three regions clearly defined: One first region approximately isothermal followed by a polytropic cooling zone and finally reaching a specific value different from zero (the tail of the Maxwellian distribution). For all the cases simulated here (mass ratios between 1000 and 100000), the convergent region of the expansion belongs to the isothermal approximation, since density approximates $\hat{n}_e = 0.5$ at the magnetic throat (the density - magnetic field relation $n(B)$ hardly varies with the mass ratio parameter). Regarding the polytropic coefficient that governs the second region, and attending to the relation

$$\hat{T}_e = \left(\frac{\hat{n}}{\hat{n}^*}\right)^{\gamma-1} \tag{24}$$

, where $\hat{n}^*$ represents a constant, the polytropic coefficient is between $\gamma = 1.45$ for $m_i/m_e = 1000$ and $\gamma = 1.57$ for $m_i/m_e = 100000$. This constant $\hat{n}^*$ is between 0.072 ($m_i/m_e = 1000$) and 0.003 ($m_i/m_e = 100000$) for the simulated cases.

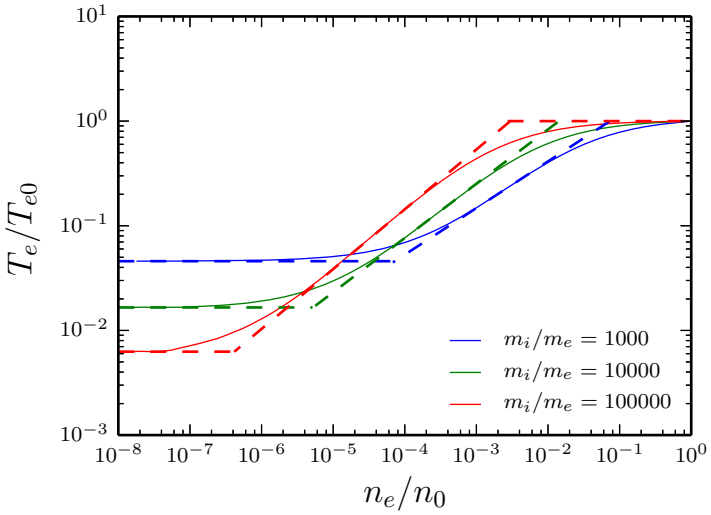

Figure 12. Electron temperature along the expansion for three different profiles m_i/m_e = [1000, 10000, 100000] and $T_{e0}/T_{i0} = 0.1$ where the expansion is from right to left. The dashed lines represent an isothermal-polytropic-isothermal approximation for each case.

VI. Conclusions and Future work

Starting from the theoretical model developed in Ref.9, this work has performed an extension of it considering Maxwellian ions instead of mono-energetic ions at the source. The parameters that drive the plasma response in this case are the ion to electron mass ratio and the ion to electron source temperature (instead of the ion to electron energy as it was in Ref.9). Furthermore, this work has made a study of the electron distribution function along the expansion, illuminating the importance of the electron confined population in regard to the electron temperature law.

Concerning the difference on the results caused by considering a Maxwellian ions distribution far upstream, Section III points out the following conclusions: There is not an appreciable difference on the potential - magnetic field relation $\phi - B$, neither on the total potential drop ϕ_∞. However, this difference becomes more remarkable for higher values of the ion to electron source temperature ratio , which is due to the wider energy dispersion band of the Maxwellian distribution function at higher ion temperatures. In addition, there is a great difference in the parallel ion temperature, that reaches a constant value far downstream, instead of dropping to zero as in the mono-energetic case. This is because the energy dispersion of the distribution is kept throughout the full expansion, and far downstream, where the magnetic field approaches zero, all this energy has been converted into parallel kinetic energy, whose dispersion is a measure of the ion parallel temperature.

Electron density and pressure have been analysed in terms of the contribution of the three different populations in which electrons can be sorted (reflected, trapped and free). This has enabled a greater comprehension about the evolution of the electron distribution function along the expansion: Confined electrons dominate the total electron density throughout the full expansion for the studied cases. This result is due to the model hypothesis itself, which assumes the presence of this population, apparently necessary to ensure simultaneously both plasma quasi-neutrality and current-free plasma beam. The contribution of the confined electrons to the total density decreases for smaller mass ratios. For them, the ambipolar electric potential is weaker and therefore the effect of potential barriers is less important. This confined population is imposed isotropic, but it is not isothermal since its temperature drops to zero along the expansion as a function of the potential- magnetic field relation. The electron cooling law given by this model can be approximated by three different regions. First, an isothermal zone (all the convergent region), then a polytropic cooling dominated by the confined electrons and finally it drops to the final lower bound limit given by the free electrons.

A parametric analysis of some interesting variables has been carried out in terms of the input parame-

ters. This includes a numerical study of fitting laws for the total potential drop and the bounded parallel electron temperature far downstream. The influence of the ion to electron source temperature ratio has been concluded to be marginal below $T_{i0}/T_{e0} = 1$.

This model could be extended modifying some hypothesis postulated here: The influence of the type of ion-electron distributions upstream, or the breaking of some conditions, such as the zero net current imposed here. In addition to modifications, the electron cooling problem can be addressed by different research lines, as simulating a transient model where particle energy is not necessarily conserved, and build a PIC code to be able to justify the existence of the trapped electron population.

Acknowledgments

The authors acknowledge fruitful discussions with Prof. Martinez-Sánchez. The work of Jaume Navarro has been funded by the Government of Spain, FPU Fellowship (Grant No. AP2010-0791). Additional support comes from the Spanish R&D National Plan (Grant No. ESP2013-41052-P)

References

[1]C. Charles and R. Boswell. Current-free double-layer formation in a high-density helicon discharge. *Applied Physics Letters*, 82(9):1356–1358, 2003.

[2]O.V. Batishchev. Minihelicon plasma thruster. *Plasma Science, IEEE Transactions on*, 37(8):1563–1571, 2009.

[3]D. Pavarin, F. Ferri, M. Manente, D. Curreli, Y. Guclu, D. Melazzi, D. Rondini, S. Suman, J. Carlsson, C. Bramanti, E. Ahedo, V. Lancellotti, K. Katsonis, and G. Markelov. Design of 50W helicon plasma thruster. In *31th International Electric Propulsion Conference*, IEPC 2009-205, 2009.

[4]C. Diaz. The VASIMR rocket. *Scientific American*, 283(5):90–97, 2000.

[5]B.W. Longmier, E.A. Bering, M.D. Carter, L.D. Cassady, W.J. Chancery, F.R.C. Díaz, T.W. Glover, N. Hershkowitz, A.V. Ilin, G.E. McCaskill, et al. Ambipolar ion acceleration in an expanding magnetic nozzle. *Plasma Sources Science and Technology*, 20:015007, 2011.

[6]Joel C Sercel. Electron-cyclotron-resonance (ECR) plasma acceleration. In *AIAA 19th Fluid Dynamics, Plasma Dynamics and Lasers Conference*, 1987.

[7]Mario Merino and Eduardo Ahedo. Influence of electron and ion thermodynamics on the magnetic nozzle plasma expansion. 2013.

[8]O. Chang J. Wang and Y. Cao. Electron–ion coupling in mesothermal plasma beam emission: Full particle pic simulations. *IEEE transactions on plasma science*, 40:230–236, 2012.

[9]M Martinez-Sanchez, J Navarro-Cavallé, and E Ahedo. Electron cooling and finite potential drop in a magnetized plasma expansion. *Physics of Plasmas (1994-present)*, 22(5):053501, 2015.